International Journal of Electrical, Electronic and Communication Sciences
ISSN: 2517-9438
Vol:13, No:2, 2019

Reduced Rule Based Fuzzy Logic Controlled Isolated Bidirectional Converter Operating in Extended Phase Shift Control for Bidirectional Energy Transfer

Anupam Kumar, Abdul Hamid Bhat, Pramod Agarwal

***Abstract*—**Bidirectional energy transfer capability with high efficiency and reduced cost is fast gaining prominence in the central part of a lot of power conversion systems in Direct Current (DC) microgrid. Preferably, under the economics constraints, these systems utilise a single high efficiency power electronics conversion system and a dual active bridge converter. In this paper, modeling and performance of Dual Active Bridge (DAB) converter with Extended Phase Shift (EPS) is evaluated with two batteries on both sides of DC bus and bidirectional energy transfer is facilitated and this is further compared with the Single Phase Shift (SPS) mode of operation. Optimum operating zone is identified through exhaustive simulations using MATLAB/Simulink and SimPowerSystem software. Reduced rules based fuzzy logic controller is implemented for closed loop control of DAB converter. The control logic enables the bidirectional energy transfer within the batteries even at lower duty ratios. Charging and discharging of batteries is supervised by the fuzzy logic controller. State of charge, current and voltage for both the batteries are plotted in the battery characteristics. Power characteristics of batteries are also obtained using MATLAB simulations.

***Keywords*—**Fuzzy logic controller, rule base, membership functions, dual active bridge converter, bidirectional power flow, duty ratio, extended phase shift, state of charge.

I. Introduction

IN modern times, the requirement of an energy efficient power electronics conversion system having inherent bidirectional energy transfer capability, low weight and reduced switching loss has increased considerably. Isolated Bidirectional Converters (BDCs) [1], [2] are fast becoming the core of common power electronics and industrial applications such as renewable energy systems, transportation vehicles industry, HVDCs [3], portable electronic equipment's, and microgrids [4], [5] which require an intermediate energy storage system [6]. For fulfilling the requirements of such systems, DAB converters were introduced in 1990 [7]. Advanced versions [8] of DAB like three phase DAB [9], multilevel DAB [10], [11], dual bridge resonant converters [12] are also developed for complimenting energy conversion purposes. Later different control techniques like EPS [13], dual phase-shift control (DPS) [14], [15] and triple phase-shift control (TPS) [16] were introduced and investigated in detail. In recent times, SiC [17] based DAB is also being developed and is leading to better efficiency and smaller size of the overall converter system [17]. Fuzzy logic controller is also being used with higher number of rules for control of DAB converter.

Some of the intrinsic attributes of DAB converters are inherent soft switching capability [18], high power density, galvanic isolation and reduced number of passive elements. Subsequently zero voltage switching operating range [19] was extended for the improvement in system efficiency. Dual active converters are also used in custom power devices like Unified Power Quality Conditioner (UPQC) [20], [21], Dynamic Voltage Restorer (DVR) [22] for facilitating bidirectional power flow and mitigation of various power quality problems. Also prior to DAB some soft switched converters have been implied in electrical vehicles [23] and studies on energy management in fuel cells have been carried out [24].

In this paper, modeling, designing of DAB and comparison based on power absorbed and power delivered by DAB in the EPS mode having battery on both the ends is performed. Reduced rule based fuzzy logic controller has been developed for the DAB system. Linguistic variables along with their membership functions are also shown along with their corresponding outputs. Sugeno fuzzy inference is used in the present work. Advantages of fuzzy logic controlled system are also discussed along with the benefits of having reduced rule base. Also a comparative analysis of EPS and SPS control modes of operation is carried out with respect to stability of operating zone and efficiency of the overall system.

Optimum duty ratio is identified from the operating zone by carrying out extensive simulations and noting the efficiency of battery converter system at desired voltage level. 3D curve of power transfer capability in EPS mode is plotted. State of charge, current, and voltage of battery are also shown in the corresponding battery characteristics. Power developed and power absorbed by batteries are also shown in power characteristics of batteries. Variation of efficiency with respect to duty ratios in EPS mode is obtained along with its power plots. By extensive simulation studies in MATLAB/Simulink and SimPowerSystems software, the above converter working in the two control modes is tested and results are obtained for a comprehensive comparative evaluation.

Anupam Kumar and Abdul Hamid Bhat are with the National Institute of Technology, Srinagar, Jammu and Kashmir, India (e-mail: kanupam310@gmail.com, bhatdee@nitsri.net).

Pramod Agarwal is with the Indian Institute of Technology, Roorkee, Uttarakhand, India (e-mail: pramgfee@iitr.ac.in).

II. Modelling and Operating Principle of DAB

A DAB consists of two DC-AC converters connected back-to-back through a high frequency transformer as shown in the schematic diagram of a single phase dual active bridge converter in Fig. 1. The inductor is a combination of primary side inductance plus the secondary side inductance referred to primary side.

A. Modelling of DAB Converter in SPS Mode

For modelling of DAB, Fig. 2 is considered.

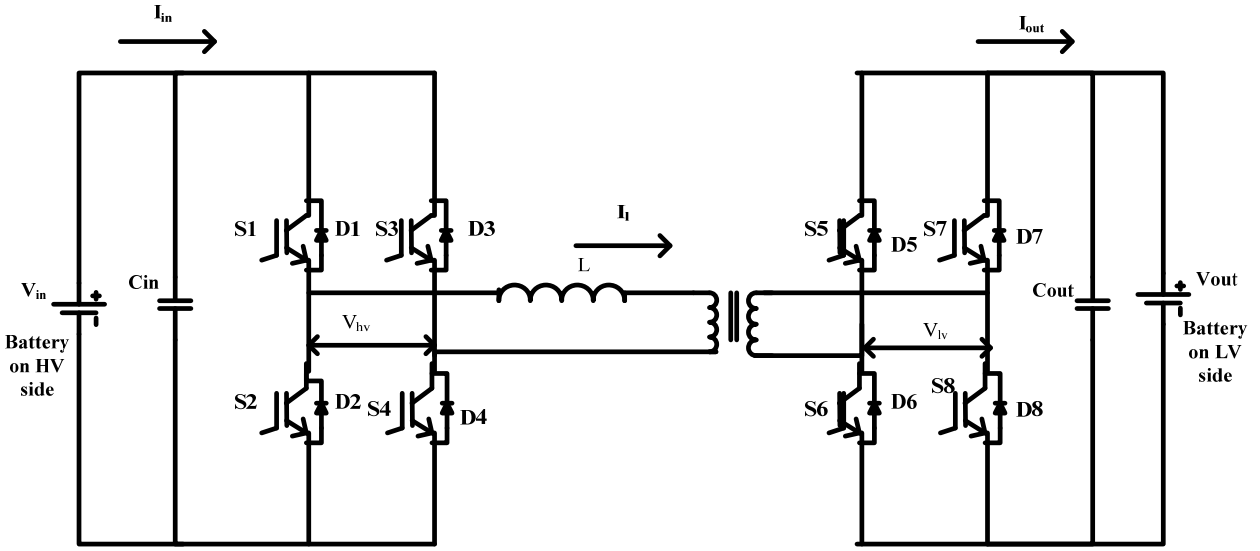

Fig.1 Power circuit diagram of single-phase DAB converter

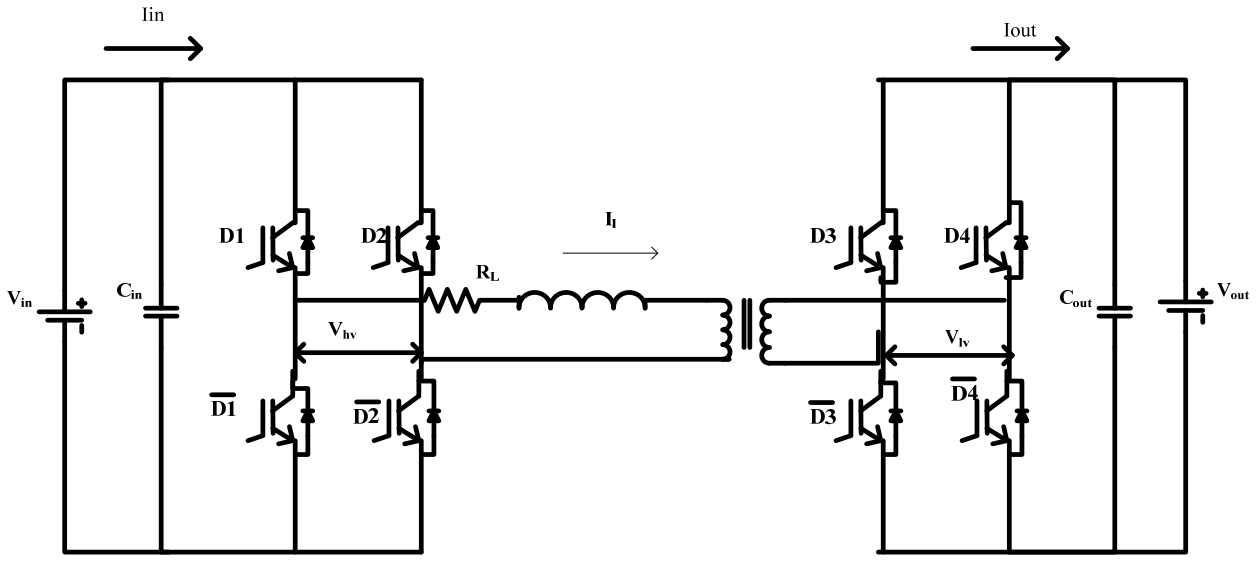

Fig. 2 Power circuit diagram of single-phase DAB converter for modeling

Converter modeling is done by applying KVL around the converter in the transformer loop: $V_{hv}=V_{Pri}$, and $V_{lv}=V_{sec}$, V_{hv}= Voltage on the high voltage side of transformer, V_{lv}= Voltage on the low voltage side of transformer.

$$V_{hv}(t)-\frac{Np}{N_s}V_{lv}(t)-R_L i_L(t)-L\frac{diL}{dt}(t)=0 \quad (1)$$

i_L= Inductor current, R_L= Resistance of leakage inductance, L= Leakage inductance, N_p= Number of turns in the Primary Side Winding. N_s= Number of turns in the Secondary Side Winding.

Now the bridge output voltages are expressed in terms of their corresponding converter switching functions as,

$$V_{hv}(t) = V_{in}(t)\ \{D_1\ (t) - D_2\ (t)\} \quad (2)$$

$$V_{lv}(t)=V_{out}(t)\{D_3(t)- D_4(t)\} \quad (3)$$

Here, $V_{in}(t)$= Input side voltage, $V_{out}(t)$= output side voltage, $D_1(t)$= Switching function of switch one, $D_2(t)$=Switching function of switch two, $D_3(t)$= Switching function of switch three, $D_4(t)$= Switching function of switch four. The square switching waveforms are expressed in sinusoidal terms by means of Fourier transform as in (4),

$$D_k(t)=\frac{1}{2}+\frac{2}{\pi}\sum_{n=0}^{\infty}\frac{1}{[2n+1]}\frac{\sin([2n+1]\{\omega_s t-\propto_k\})}{[2n+1]}\text{k=0,1,2} \quad (4)$$

where, $\omega_s$is the switching frequency of the square wave and $\propto_k$ is the phase delay of waveform with respect to a reference phasor.

Now for simplification of whole calculation, the infinite Fourier series is truncated to first 'N' harmonics. Thus, the switching function becomes

$$D_k(t)=\frac{1}{2}+\frac{2}{\pi}\sum_{n=0}^{N}\frac{1}{[p]}\frac{\sin([p]\{\omega_s t-\propto_k\})}{[p]} N\geq 0\ ,\ k=1,2,3\ldots,$$
$$p=2n+1 \quad (5)$$

As DAB has four switches, four switching functions are required to be formulated. Thus following assumptions have to be made.

a) Switch D_1 is taken as reference phasor.
b) The phase difference between complementary pair of switches is 180°.
c) The phase difference between primary side voltage and secondary side voltage is ∅.

Thus, the following switching functions are obtained:

$$D_1(t)=\frac{1}{2}+\frac{2}{\pi}\sum_{n=0}^{N}\frac{1}{[p]}\frac{\sin([p]\{\omega_s t\})}{[p]} p=2n+1 \quad (6)$$

n= integers representing the number of harmonics

$$D_2(t)=\frac{1}{2}+\frac{2}{\pi}\sum_{n=0}^{N}\frac{1}{[p]}\frac{\sin([p]\{\omega_s t-\pi\})}{[p]} \quad (7)$$

$$D_3(t)=\frac{1}{2}+\frac{2}{\pi}\sum_{n=0}^{N}\frac{1}{[p]}\frac{\sin([p]\{\omega_s t-\emptyset\})}{[p]} \quad (8)$$

$$D_4(t)=\frac{1}{2}+\frac{2}{\pi}\sum_{n=0}^{N}\frac{1}{[p]}\frac{\sin([p]\{\omega_s t-\emptyset-\pi\})}{[p]} \quad (9)$$

Substituting the values of V_{Pri} and V_{sec} from (2) and (3) in (1), we get:

$$R_L i_L(t)+L\frac{di_L}{dt}(t)=Vin(t)\{D_1(t)-D_2(t)\}-\frac{N_p}{N}Vout(t)\{D_3(t)-D_4(t)\} \quad (10)$$

Now substituting the values of D_1, D_2, D_3, D_4 in (10), we get:

$$R_L i_L(t)+L\frac{di_L}{dt}(t)=Vin(t)\{\frac{4}{\pi}\sum_{n=0}^{N}\frac{\sin([p]\{\omega_s t\})}{[p]}\}-\frac{N_p}{N_s}Vout(t)\{\frac{4}{\pi}\sum_{n=0}^{N}\frac{\sin([p]\{\omega_s t-\emptyset\})}{[p]}\} \quad (11)$$

Now for determining the value of N, analytical power flow expression and harmonic power summation are compared.

Analytical power flow is given by, $P=\frac{N_p V_{in} V_{out}\emptyset(\Pi-\emptyset)}{N_s w_s L\,\Pi}$; here ∅ is phase shift between the two bridges, and L is the inductance between the bridges.

Harmonic power flow summation is given by,

$$P_{sec}=\frac{8}{\pi^2}V_{in}V_{out}\frac{Np}{N_s}\sum_{n=0}^{N}\frac{1}{[p]^3}\frac{\sin([p]\emptyset)}{\omega_s L} \quad p=2n+1$$

For N= 3, the difference between the analytical power flow and harmonic power flow summation is less than 0.01%. Therefore, N=3 is used for the analysis.

Expressing (11) in phasor domain:

$$R_L i_L(t)+L\frac{di_L}{dt}(t)=\{R_{\text{橿}}+j[p]\omega_s L\}I_{L[p]}$$
$$V_{P\,ri}[2n+1]+\frac{N_p}{N_s}V_{sec}=\frac{4}{\pi}\frac{1}{[p]}\{Vin\angle 0-\frac{N_p}{N_s}Vout\angle-[p]\emptyset\}$$

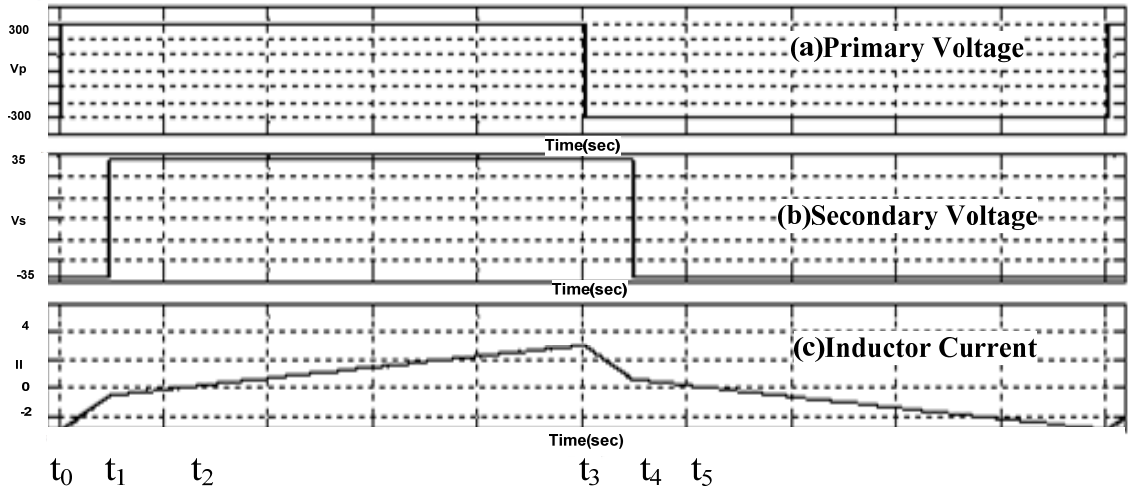

Fig. 3 (a) Primary voltage (b) Secondary voltage (c) Inductor current for forward power flow

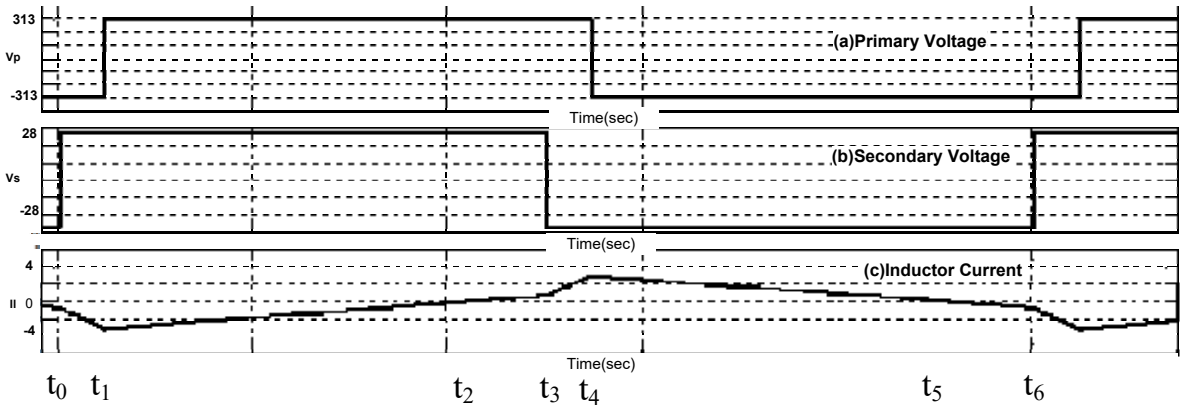

Fig. 4 (a) Primary voltage (b) Secondary voltage (c) Inductor current for reverse power flow

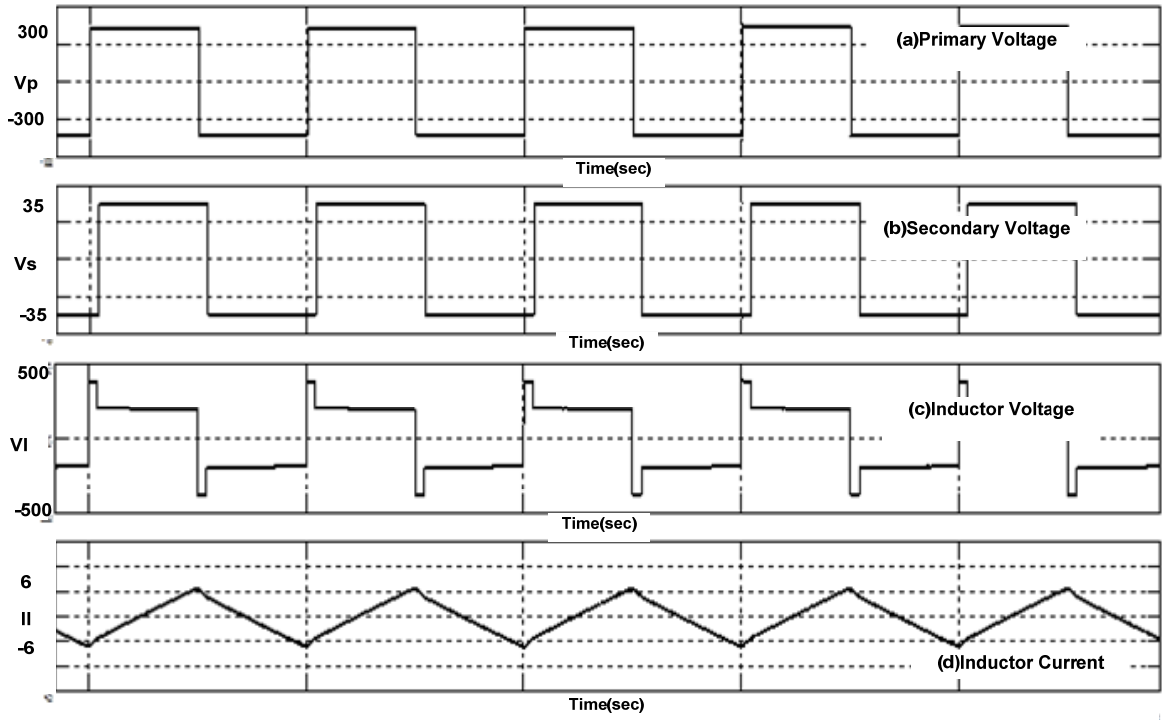

Fig. 5 (a) Simulated Primary voltage, (b) Secondary voltage, (c) Inductor voltage, (d) Inductor current for forward power flow

A modified (11) is obtained which is written below:

$$\{R_L + j[2n+1]\omega_s L\}I_{L[2n+1]} = \frac{4}{\pi}\frac{1}{[2n+1]}\{Vin\angle 0 - \frac{Np}{N_s}Vout\angle - [2n+1]\emptyset\} \quad (12)$$

$$\Rightarrow I_{L[2n+1]} = \frac{\frac{4}{\pi}\frac{1}{[2n+1]}\{Vin\angle 0 - \frac{Np}{N_s}Vout\angle -[2n+1]\emptyset\}}{\{R_L + j[2n+1]\omega_s L\}I_{L[2n+1]}} \quad (13)$$

Now this phasor domain expression of inductor current is expressed in time domain.

$$i_L(t) = \frac{4}{\pi}\sum_{n=0}^{N}\frac{1}{[2n+1]}\left\{\frac{Vin}{Z[n]}\sin([2n+1]\omega_s t - \theta_n)\right\} - \frac{Vout}{Z[n]}\frac{Np}{N_s}\sin([2n+1]\{\omega_s t - \emptyset\} - \theta_n) \quad (14)$$

$|Z[n]| = \sqrt{{R_L}^2 + ([2n+1]\omega_s L)^2}$ here Z[n]= Impedance at nth harmonic.

$$\theta_n = \tan^{-1}\frac{[2n+1]\omega_s L}{R_L}$$

In SPS mode, transmitted power is given by

$$P = \frac{nV_1V_2D(1-D)}{2LF_S} \quad (15)$$

where, V_1= Primary side voltage, V_2= Secondary side voltage, n= Transformation ratio of isolation transformer, D= Duty ratio corresponding to outer phase shift between the two bridges.

The waveform for DAB working in SPS control mode for forward power flow mode is shown in Fig. 3. Similarly, the waveforms can be seen in Fig. 4 for the reverse power flow mode. The conduction of various devices in charging as well as discharging mode is shown in Tables I A and B. Also the switch conduction table is made considering Figs. 3 and 4 for Fig. 1. Also the primary voltage, secondary voltage, inductor voltage and inductor current are shown in Figs. 5 and 6 for forward as well as reverse conduction mode respectively.

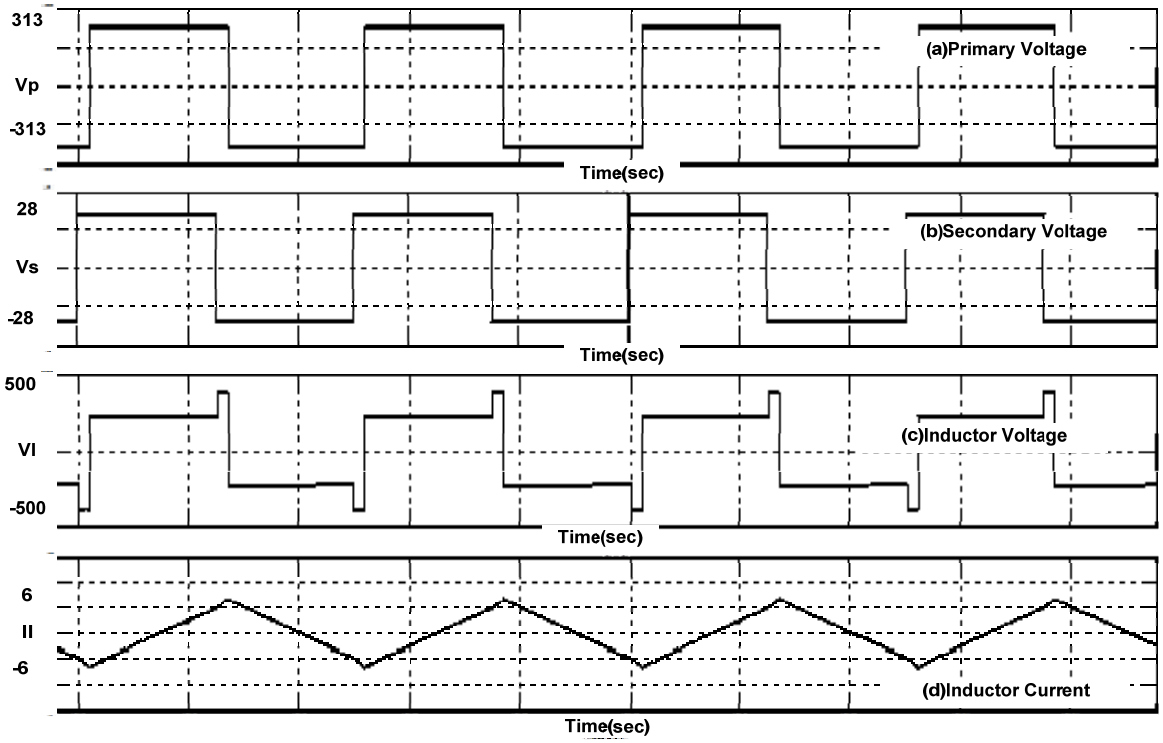

Fig. 6 (a) Simulated primary voltage (b) Secondary voltage, (c) Inductor voltage, (d) Inductor current for reverse power flow

The unified transmission power is defined as

$$P_t = 4D(1-D) = \frac{P}{P_N} \text{ where} P_N = \frac{nV_1V_2}{8LF_s} \qquad (16)$$

The 3-D graph of this unified transmission power is shown in Fig. 7. Also backflow power in SPS mode is expressed as:

$$P_{bf} = \frac{nV_1V_2\,[a+(2D-1)]^2}{16f_s\,L(a+1)}$$

B. EPS Control

EPS control mode is applied for overcoming the deficiencies in SPS control strategy (SPS control mode has lower efficiency; zero voltage switching operating range is small and has a higher circulating power). In EPS control, the switch pairs in one bridge are provided with inner phase shift while other switch pairs are switched as before with outer phase shift only. This results in the primary side voltage becoming a three level wave and secondary side waveform remains a two level wave having 50% duty ratio. In reverse conduction mode, the waveshapes of both the voltages are interchanged. The operating principle and performance of EPS has been discussed by many researchers [2], [13]. Also the waveforms for EPS technique in forward and reverse conduction mode are shown in Figs. 8 and 9.

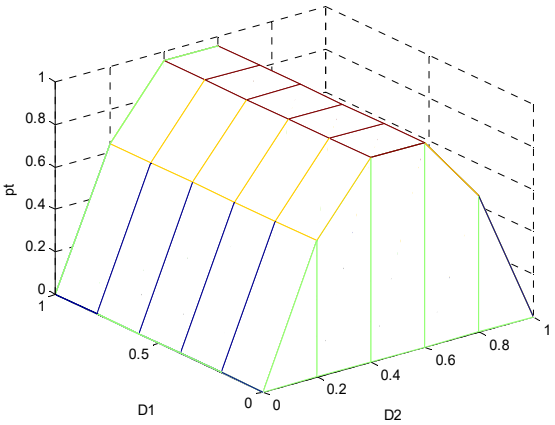

Fig. 7 Relation curve of unified transmission power with duty ratio $D_1 = D_2 = D$

The conduction of various devices in charging as well as discharging mode is shown in Tables II A and B. These tables are obtained from Figs. 8 and 9.

TABLE I A
DEVICE CONDUCTION TABLE FOR FORWARD POWER FLOW IN SPS MODE

Time interval	Device conducting in primary bridge	Device conducting in secondary bridge
t_0-t_1	D1-D4	D5-D8
t_1-t_2	S1-S4	S5-S8
t_2-t_3	S1-S4	D6-D7
t_3-t_4	D2-D3	D6-D7
t_4-t_5	S2-S3	S7-S6
t_5-t_6	S2-S3	D5-D8

TABLE I B
DEVICE CONDUCTION TABLE FOR REVERSE POWER FLOW IN SPS MODE

Time interval	Device conducting in primary bridge	Device conducting in secondary bridge
t_0-t_1	D2-D3	D6-D7
t_1-t_2	S2-S3	S7-S6
t_2-t_3	D1-D4	S7-S6
t_3-t_4	D1-D4	D5-D8
t_4-t_5	S1-S4	S5-S8
t_5-t_6	D2-D3	S5-S8

The unified transmission power in case of EPS control mode is expressed as

$$P_{te} = 4D_2(1-D_2) + 2D_1(1-D_1-2D_2)] = \frac{P}{P_N} \quad (17)$$

where,

$$P_N = \frac{nV_1V_2}{8Lf_s}$$

where V_1=Primary side voltage, V_2=Secondary side voltage, n=Transformation ratio of isolation transformer, D_1=Inner phase shift duty ratio in primary bridge, D_2=Outer phase shift duty ratio between primary bridge voltage and secondary bridge voltage, f_s=Switching frequency, L=Leakage inductance of primary plus referred value of secondary side leakage inductance on primary side.

From Fig. 8, low-frequency average model of the system can be developed keeping in mind the fact that the average current of the inductor over one switching period should be zero.

TABLE II A
DEVICE CONDUCTION TABLE FOR FORWARD POWER FLOW IN EPS MODE

Time interval	Device conducting in primary bridge	Device conducting in secondary bridge
t_0-t_1	D2-D3	D6-D7
t_1-t_2	S2-S3	S7-S6
t_2-t_3	D1-D4	S7-S6
t_3-t_4	D1-D4	D5-D8
t_4-t_5	S1-S4	S5-S8
t_5-t_6	D2-D3	S5-S8

TABLE II B
DEVICE CONDUCTION TABLE FOR REVERSE POWER FLOW IN EPS MODE

Time interval	Device conducting in primary bridge	Device conducting in secondary bridge
t_0-t_1	D1-D3	S7-S6
t_1-t_2	D1-D3	S6-D8
t_2-t_3	S1-S4	S8-D6
t_3-t_4	S1-S4	S5-S8
t_4-t_5	D2-S4	S5-S8
t_5-t_6	D2-S4	S5-D7
t_6-t_7	S2-S3	D5-S7
t_7-t_8	S2-S3	S7-S6

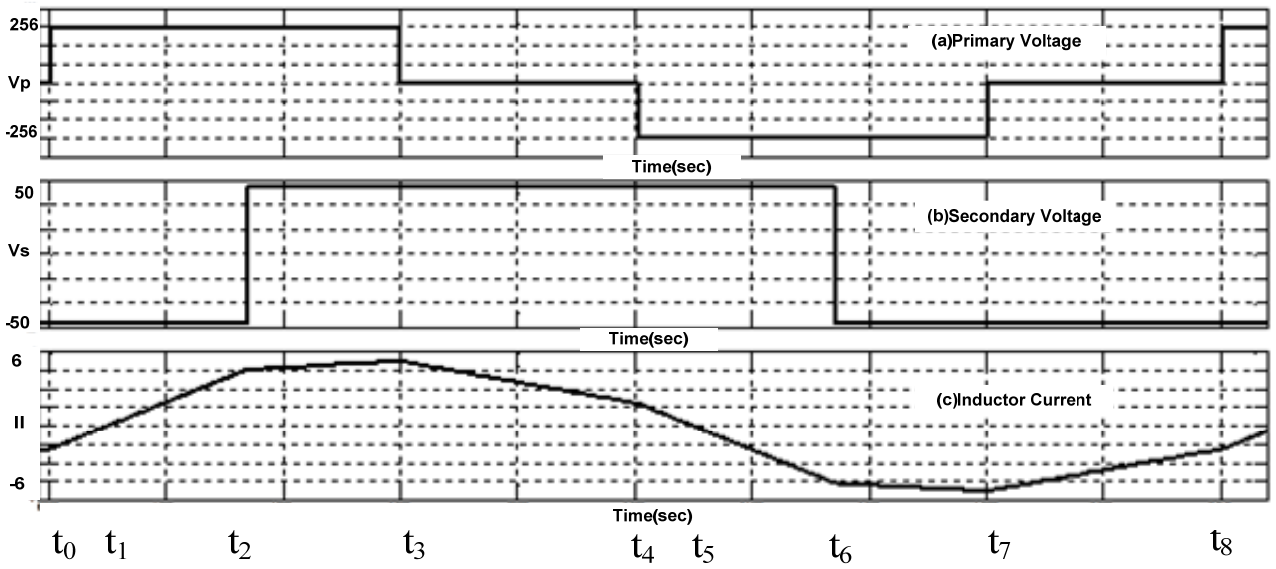

Fig. 8 (a) Simulated Primary voltage (b) Secondary voltage (c) Inductor current for forward power flow

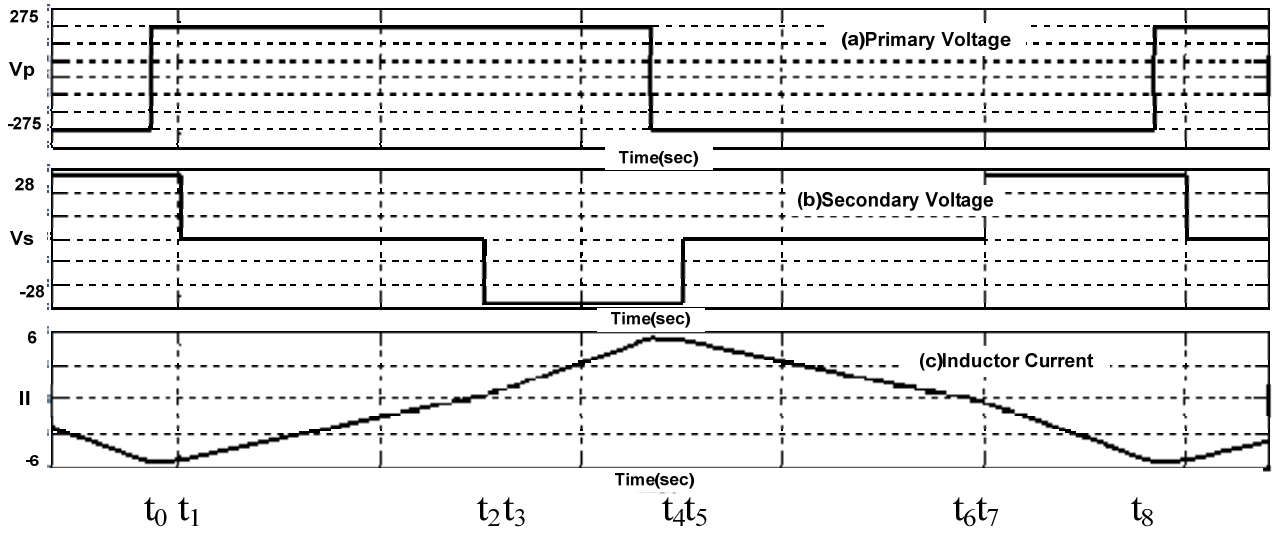

Fig. 9 (a) Simulated Primary voltage (b)Secondary voltage (c) Inductor current for reverse power flow

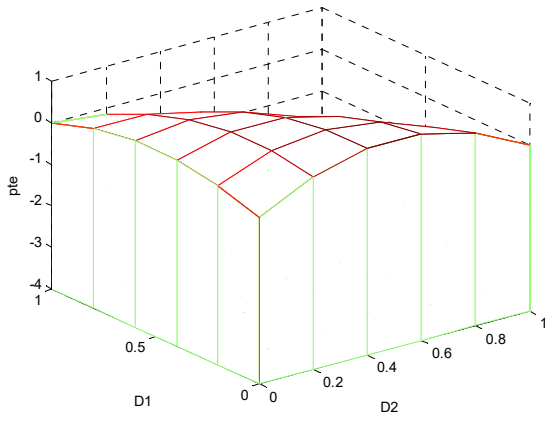

Fig. 10 Relation curve of unified transmission power with duty ratio $D_1=D_2=D$

Values of inductor current at various instances of time are expressed below: For Fig. 8, corresponding values of inductor current at different instants of time are as:

$$i_L(t_7) = -\frac{nV_2}{4Lf_s}[a(1-D_1)+(2D_1+2D_2-1)] \quad (18)$$

$$i_L(t_1) = -\frac{nV_2}{4Lf_s}[a(1-D_1)+(2D_2-1)] \quad (19)$$

$$i_L(t_2) = -\frac{nV_2}{4Lf_s}[a(2D_1+2D_2-1)+1] \quad (20)$$

$f_s=1/(2T_{hs})$ is switching frequency,$a=V_1/nV_2$

$$i_{max}=|i_L(t_7)| = -\frac{nV_2}{4Lf_s}[a(1-D_1)+(2D_1+2D_2-1)] \quad (21)$$

The transmitted power is expressed as:

$$P=\frac{nV_1V_2}{2Lf_s}[D_2(1-D_2)+\frac{1}{2}D_1(1-D_1-2D_2)] \quad (22)$$

3D-curve of Unified Transmission power is plotted in Fig. 10.

III. Reduced Rule Based Fuzzy Logic Control Of DAB

A. Fuzzy Logic Controller for SPS Mode

Fuzzy logic controller is used in finding solutions for problems in which mathematical calculations are tedious and lengthy. In systems where the mathematical modeling of system is complex and a large number of variables are involved, fuzzy logic can be used due to its simple and sophisticated nature. Also due to its high sensitivity towards system variations and a remarkable feature of representing simple human thinking towards a problem, fuzzy logic controller is preferred over conventional PI controller.

Sugeno fuzzy model is implied in the present work for formation of fuzzy logic based closed loop controller. As the Sugeno fuzzy inference provides a reduced computational burden and is quite versatile in nature, it is preferred over Mamdani fuzzy inference. The fuzzy logic closed loop controller is shown in Fig. 11. From Fig. 11, it becomes clear that the output voltage is compared with the reference voltage, thereafter the error and the derivative of error is processed through the fuzzy logic controller. A square wave of frequency 20 KHz and duty ratio of 50% is generated and is given along with the output of fuzzy logic controller to phase shift modulator. As the scheme consists of two batteries, two fuzzy logic controllers are required for closed loop control of the whole system.

The fuzzy logic system consists of three major components; namely fuzzification, decision making and defuzzification.

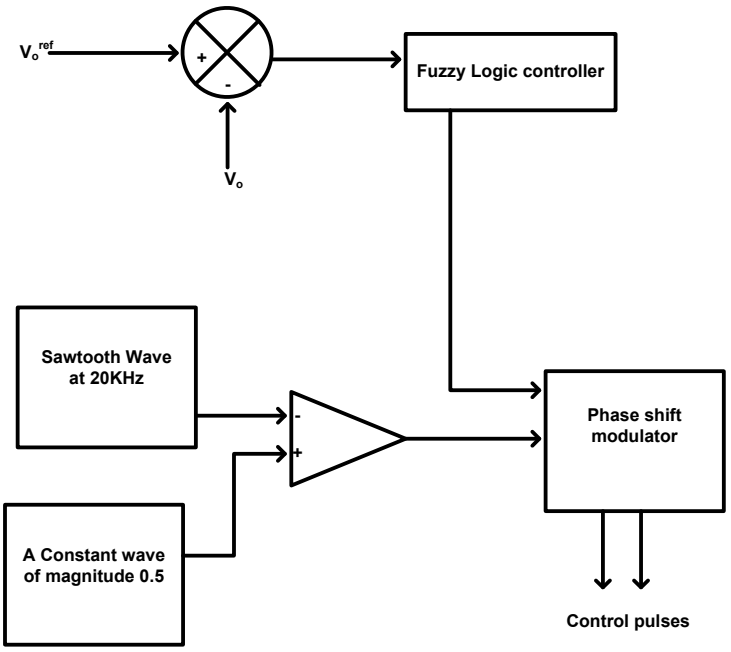

Fig. 11 Fuzzy logic based closed loop controller

Fuzzification: Under the process of fuzzification, input variables (error (e) and change in error (de)) and output variables are converted into fuzzified signals with their recognition done by their levels of membership in fuzzy sets. The numerical variables are converted into linguistic variables, and the following two fuzzy levels or sets are selected:

1. ZE: Zero
2. PB: Positive big

Application of two fuzzy sets reduces the number of rules to 4. This further eases the computational burden on the system.

The fuzzy control implemented here utilises triangular membership functions for input linguistic variables. The membership functions for error 'e', change in error 'de' and output for both the controllers are shown in Figs. 12 and 13. In Fig. 12 (a) it is depicted that error 'e' has two membership functions namely ZE and PB. Membership function 'ZE' varies from 0 to 6.5 and PB varies from 4.5 to 35. The output actuating signals ZE and PB are assigned values of 0.1 and 20.5 respectively. This fuzzy logic controller is used for the battery at the LV (low voltage) side during the forward mode of operation. The membership grade of each input is assigned between the range of 0 to 1. The linguistic variable change in error 'de' is same as the linguistic variable 'e' and has the same membership functions.

For the fuzzy logic controller used for the battery on the HV (high voltage) side during the reverse mode of operation, the linguistic variables are shown in Fig. 13 (a) where for 'e', ZE varies from 0 to 295, and PB varies from 270 to 304. For linguistic variable 'de' shown in Fig. 13 (b), ZE varies from 0 to 6.5, and PB varies from 4.5 to 35. The output actuating signals ZE and PB are assigned values of 0.1 and 17 respectively and are shown in Fig. 13 (c).

Decision making: In Sugeno implication method, the output membership functions are either constant or have a linear relationship with output. The input is associated to the output by If-Then principle. As the membership functions are reduced to two for both error and change in error, a total of 4(2*2) rules are possible. Fuzzy logic control rules are shown in Table III.

TABLE III
REDUCED RULE BASE TABLE FOR FUZZY LOGIC CONTROLLER

e \ de	ZE	PB
ZE	ZE	PB
PB	PB	PB

The defuzzifier converts the output of fuzzy logic controller which is of the form of linguistic variables into crisp solution variable. Basically it is the reverse process of fuzzification.

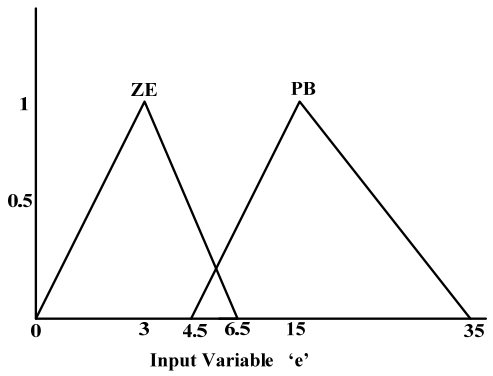

(a)

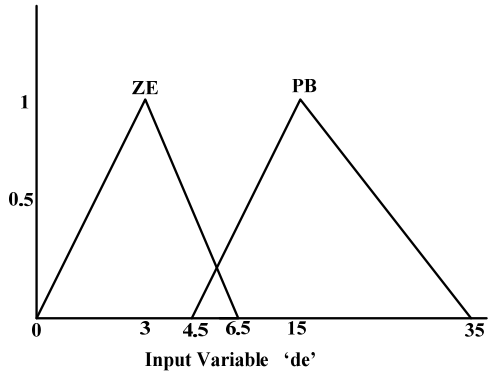

(b)

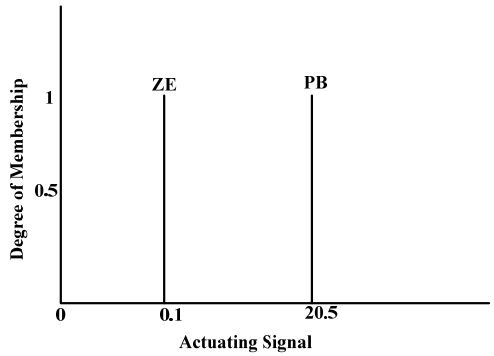

(c)

Fig. 12 (a) Input variable 'e' (b) Input variable change in error 'de' (c) Actuating Signal for fuzzy logic controller in SPS mode for battery at LV side

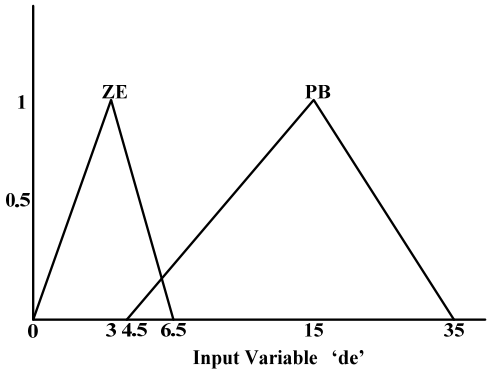

(b)

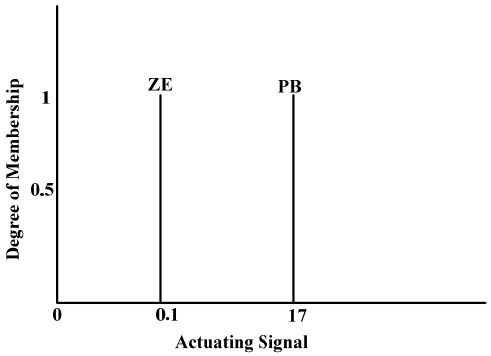

(c)

Fig. 13 (a) Input variable 'e' (b) Input variable change in error 'de' (c) Actuating Signal for fuzzy logic controller in SPS mode for battery at HV side

B. Fuzzy Logic Controller for EPS Control Mode

The above discussed Fuzzy logic based closed loop controller is used in the SPS control mode. The membership functions of linguistic variables in the process of fuzzification are changed so that the above controller is implemented in EPS control mode.

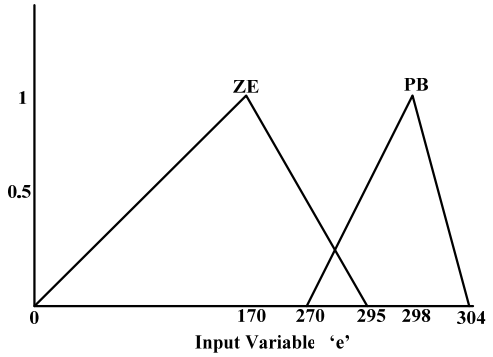

(a)

Fuzzification in EPS mode: The membership functions for error 'e', change in error 'de' and output for both the controllers are shown in Figs. 14 and 15. From Fig. 14 it can be seen that error 'e' consists of two membership functions namely ZE and PB. Membership function 'ZE' varies from 0 to 19 and PB varies from 18 to 50. The membership grade of each input is assigned value within the range of 0 to 1. For linguistic variable 'de' shown in Fig. 14 (b), ZE varies from -1 to 0, and PB varies from -0.5 to 50. The output actuating signals ZE and PB are assigned values of 1.5 and 35 respectively.

For the fuzzy logic controller used for the battery on the HV side during the reverse mode of operation, the linguistic variables are shown in Fig. 15 (a) where for 'e', ZE varies from -0.8 to 17.5 and PB varies from 2.64 to 350. The linguistic variable change in error, 'de' is similar to the linguistic variable 'e' and has the same membership functions.

The output actuating signals ZE and PB are assigned values of 9 and 35 respectively shown in Fig. 15 (c).

Decision making and defuzzification for fuzzy logic controller in EPS mode are similar to that in SPS mode.

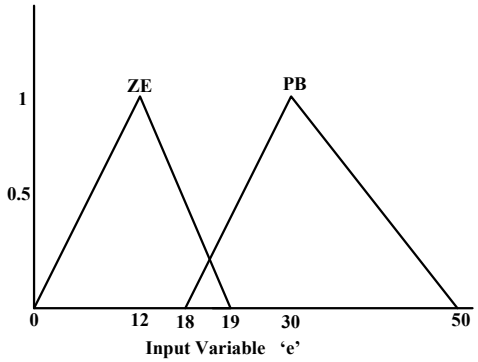

(a)

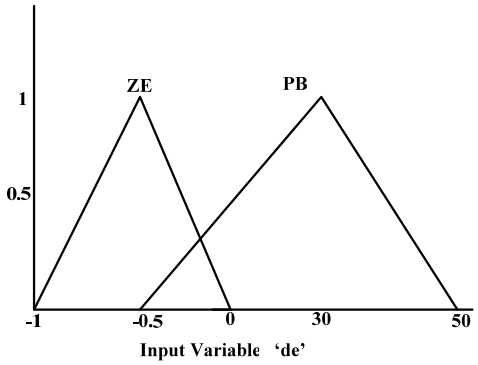

(b)

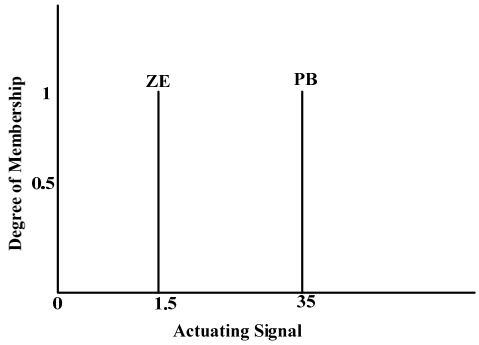

(c)

Fig. 14 (a) Input variable 'e' (b) Input variable change in error 'de' (c) Actuating Signal for fuzzy logic controller in EPS mode for battery at LV side

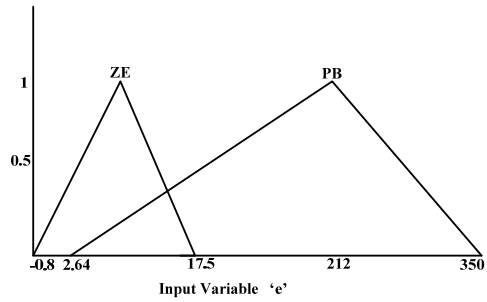

(a)

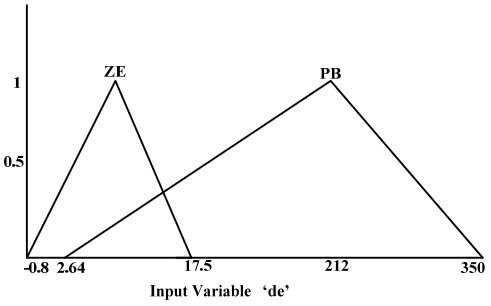

(b)

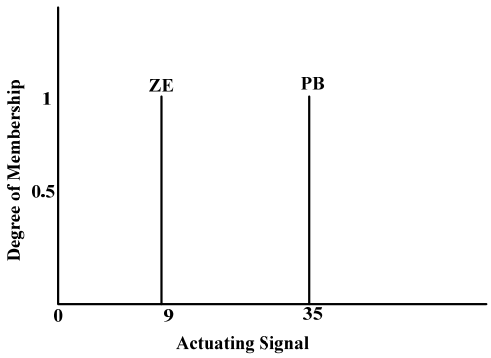

(c)

Fig. 15 (a) Input variable 'e' (b) Input variable change in error 'de' (c) Actuating Signal for fuzzy logic controller in EPS mode for battery at HV side

IV. Identification of Operating Zone

A. Operating Zone Selection for SPS Mode of DAB

For SPS control mode of DAB, duty ratio is varied in the range of 0.02 to 0.958. In the entire range, it can be observed that the battery voltage attains the value of 35 Volts at duty ratios of 0.02 and at 0.958 respectively in the forward conduction mode. But the efficiency is highest at the duty ratio of 0.02. Also the entire operating range is stable and none of the duty ratio results in unstable operation. Unstable operation means that the waveforms of secondary voltage no-longer remain a square wave having a duty ratio 0.5. The duty ratio along with efficiency and voltage is shown in Table IV A. The graph between efficiency and duty ratio is obtained and is shown in Fig. 16. After this, the duty ratio is varied for reverse conduction mode. From the table it can be seen that the efficiency varies widely over the entire operating range (D = 0.032 to0.89). Wide variations in voltage are observed over the entire operating range. Waveforms are stable at all duty ratios but best results are obtained at a duty ratio of 0.82. Also the voltage remains fixed at 313.2 V. The duty ratio variation with efficiency is shown in Table IV B. Also the graph for above variation is plotted in Fig. 17. So, the duty ratio of 0.02 is selected for converter operation in forward conduction mode while the duty ratio of 0.82 is selected for converter operation in reverse conduction mode.

TABLE IV A
EFFICIENCY AND DUTY RATIO FOR DAB WITH SPS CONTROL IN FORWARD MODE

Duty Ratio	Input Power (P_{in} in VA)	Storage Power (P_s in VA)	Efficiency (η in %)	Output Voltage (V_{out} in V)
D_2=0.02	64	45.8	71.56	35.09
D_2=0.1	230.5	214.5	93.05	45.59
D_2=0.25	557	536	96.22	59.12
D_2=0.35	716.2	685	95.64	64.14
D_2=0.45	782.5	739	94.44	64.71
D_2=0.50	792.5	741.8	93.60	64.72
D_2=0.75	562.5	489	86.93	57.3
D_2=0.85	352.5	277	78.58	48.62
D_2=0.95	135	65.7	48.66	36.61
D_2=0.958	119.5	51	42.677	35.5

TABLE IV B
EFFICIENCY AND DUTY RATIO FOR DAB WITH SPS CONTROL IN REVERSE MODE

Duty Ratio	Input Power (P_{in} in VA)	Storage Power (P_s in VA)	Efficiency (η in %)	Output Voltage (V_{out} in V)
D_2=0.032	42.8	20.5	47.89	307.7
D_2=0.5	66.8	44.8	67.0658	310.2
D_2=0.82	102.7	83.8	81.59	313.2
D_2=0.1	124.2	98	78.90	315.1
D_2=0.25	227	193	85.022	323.9
D_2=0.35	255.7	217.1	84.90	325.8
D_2=0.45	267	223.6	83.74	326.3
D_2=0.50	268.5	222.6	82.79	326.5
D_2=0.75	232.1	175.2	75.48	322.2
D_2=0.89	145.1	83.2	57.33	313.7

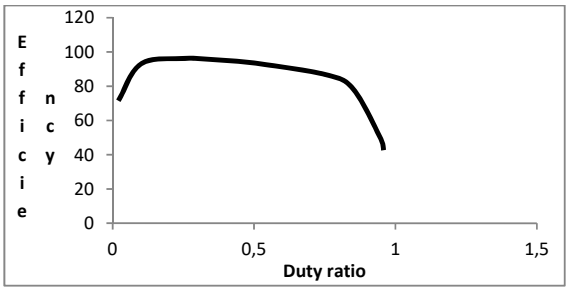

Fig. 16 Graph between efficiency and duty ratio for DAB with SPS control in forward mode with fuzzy logic controller

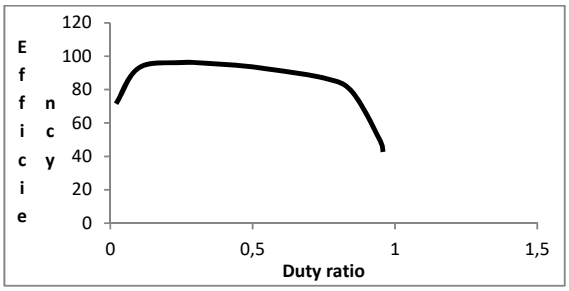

Fig. 17 Graph between efficiency and duty ratio for DAB with SPS control in reverse mode with fuzzy logic controller

B. Operating Zone Selection for EPS Mode of DAB

In case of EPS control mode, the duty ratio is varied in three range, first inner phase shift is assigned three values namely, D_1 = 0.3, 0.5 & 0.75. After this the outer phase shift (D_2) is varied from 0.1 to0.95. The variation of efficiency with respective duty ratios is shown in Tables V A-C.

TABLE V A
EFFICIENCY AND DUTY RATIO FOR DAB WITH EPS CONTROL IN FORWARD MODE FOR D_1=0.3.

Duty Ratio	Input Power (P_{in} in VA)	Storage Power (P_s in VA)	Efficiency (η in %)	Output Voltage (V_{out} in V)
D_2=0.1	79.422	83.8	94.77	30.68
D_2=0.25	21.66	24.45	88.58	32.45 (Reversal)
D_2=0.35	20.02	17.41	86.96	34.72
D_2=0.45	70.4	66.98	95.14	38.75
D_2=0.5	99.10	94.85	95.71	40.76
D_2=0.75	252.8	240.5	95.13	49.20
D_2=0.85	258.5	242.40	93.77	49.21
D_2=0.95	216.21	197.04	91.13	46.85

TABLE V B
EFFICIENCY AND DUTY RATIO FOR DAB WITH EPS CONTROL IN FORWARD MODE FOR D_1=0.5

Duty Ratio	Input Power (P_{in} in VA)	Storage Power (P_s in VA)	Efficiency (η in %)	Output Voltage (V_{out} in V)
D_2=0.1	66.3	72.3	91.70	31.04 (Reversal)
D_2=0.25	30.90	26.48	85.69	35.57 (Reversal)
D_2=0.35	118.05	113.18	95.875	41.99
D_2=0.45	228.2	220.8	96.75	48.18
D_2=0.483	267.23	258.7	96.70	50.08
D_2=0.5	288	278.2	96.59	51.03
D_2=0.75	416.2	391.8	94.13	56.10
D_2=0.88	346.6	315.2	90.94	52.53
D_2=0.90	275.6	89.48	89.48	50.84

TABLE V C
EFFICIENCY AND DUTY RATIO FOR DAB WITH EPS CONTROL IN FORWARD MODE FOR D_1=0.75.

Duty Ratio	Input Power (P_{in} in VA)	Storage Power (P_s in VA)	Efficiency (η in %)	Output Voltage (V_{out} in V)
D_2=0.1	42.7	53.5	79.81	31.61
D_2=0.25	291.5	282.22	96.81	57.93
D_2=0.35	439.28	424.5	96.64	57.31
D_2=0.45	540.4	517.85	95.827	61.08
D_2=0.5	569.5	542.5	95.25	61.89
D_2=0.75	485	438.5	90.412	57.93
D_2=0.85	354	304.5	86.01	52.24
D_2=0.88	307.5	257.8	83.88	50.04
D_2=0.90	275	225.5	82	48.41

It can be easily manifested that EPS control mode definitely has a wider operating range than SPS control mode (resultant of inner phase shift). From the tables, it can be observed that EPS control mode does not have any unstable duty ratios. Also from the table it can be observed that at some duty ratios (D_1 = 0.3, D_2 = 0.1), (D_1 = 0.5, D_2 = 0.1, 0.25), there is reversal in power conduction direction happening. Reversal in power flow direction implicates that the power flow is from storage

element to the source in case of forward power flow. The duty ratio $D_1 = 0.5$, $D_2 = 0.483$ is selected as operating duty ratio as efficiency of converter operation (96.70%) is highest at this value and desired voltage level of 50V is achieved. The graph between efficiency and duty ratios is plotted in Figs. 18 (a)-(c) for all the duty ratios.

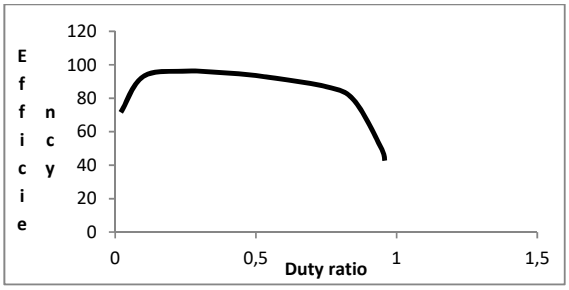

Fig. 18 (a) Graph between efficiency and duty ratio for DAB with EPS control in forward mode at duty ratio of $D_1 = 0.3$, $D_2 = 0.1$ to 0.95

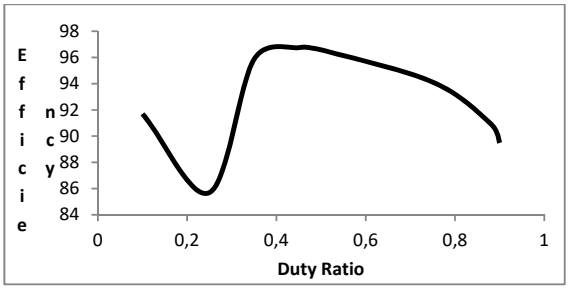

Fig. 18 (b) Graph between efficiency and duty ratio for DAB with EPS control in forward mode at duty ratio of $D_1 = 0.5$, $D_2 = 0.1$ to 0.90

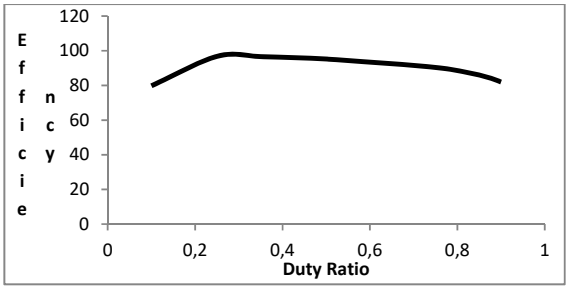

Fig. 18 (c) Graph between efficiency and duty ratio for DAB with EPS control in forward mode at duty ratio of $D_1 = 0.75$, $D_2 = 0.1$ to 0.90

In EPS control mode for reverse power flow again three duty ratios are selected namely, $D_1 = 0.3$, 0.5 & 0.75. After this the outer phase shift (D_2) is varied from 0.1 to 0.95. The variation of efficiency with respective duty ratios is shown in Tables VI A-C.

From Tables VI A-C, it is evident that the EPS control mode for reverse power flow does not have any unstable point. Reversal of power flow happens at duty ratio of $D_2 = 0.1$ for $D_1 = 0.5$, and at $D_2 = 0.25$ for $D_1 = 0.3$. As the efficiency is highest at $D_1 = 0.5$ and $D_2 = 0.43$, and the desired voltage level of 275 V is achieved. Hence this is taken as the operating duty ratio.

TABLE VI A
EFFICIENCY AND DUTY RATIO FOR DAB WITH EPS CONTROL IN REVERSE MODE FOR $D_1 = 0.3$

Duty Ratio	Input Power (P_{in} in VA)	Storage Power (P_s in VA)	Efficiency (η in %)	Output Voltage (V_{out} in V)
D_2=0.25	47.75	30.57	64.35	263.66 (Reversal)
D_2=0.35	4.4	13.52	31.544	264.9
D_2=0.45	34.7	53.88	64.402	268.40
D_2=0.5	52.75	73.43	71.83	270.1
D_2=0.65	105.5	129.1	81.72	274.9
D_2=0.75	127.2	153.2	83.02	277
D_2=0.85	121.5	154.8	78.49	275.82
D_2=0.95	107.5	138.28	77.75	275.3

TABLE VI B
EFFICIENCY AND DUTY RATIO FOR DAB WITH EPS CONTROL IN REVERSE MODE FOR D_1=0.5

Duty Ratio	Input Power (P_{in} in VA)	Storage Power (P_s in VA)	Efficiency (η in %)	Output Voltage (V_{out} in V)
D_2=0.1	112	99	88.39	261.9 (Reversal)
D_2=0.25	3.5	18.38	19.04	265.3
D_2=0.35	65.3	81.7	79.80	271.3
D_2=0.43	109.65	128.97	85.02	275.5
D_2=0.45	119.5	139.52	85.65	276.3
D_2=0.5	142	164.7	86.21	278.4
D_2=0.65	178.7	205.75	86.85	281.6
D_2=0.75	179.2	207.57	85.508	281.7
D_2=0.85	162.5	196.05	82.88	280.3
D_2=0.95	126.5	162	77.97	276.8

TABLE VI C
EFFICIENCY AND DUTY RATIO FOR DAB WITH EPS CONTROL IN REVERSE MODE FOR $D_1 = 0.75$

Duty Ratio	Input Power (P_{in} in VA)	Storage Power (P_s in VA)	Efficiency (η in %)	Output Voltage (V_{out} in V)
D_2=0.1	17.8	30.8	57.8	266.7
D_2=0.25	145.3	162.87	89.21	278.6
D_2=0.35	191.2	212.93	90.26	282.7
D_2=0.45	213.8	239.65	89.21	284.7
D_2=0.5	32.8	77.3	42.43	268.2
D_2=0.65	212.6	246.275	86.32	284.5
D_2=0.75	190.8	228.05	83.66	282.6
D_2=0.85	149.2	189.75	78.63	275
D_2=0.916	106.75	149.4	71.45	275.2
D_2=0.95	79.9	122.95	64.99	272.8

The graph between efficiency and duty ratio is plotted in Figs. 19 (a)-(c) for all the duty ratios.

V. PERFORMANCE EVALUATION

A. SPS Technique

The proposed, reduced rule based fuzzy logic controller is simulated for the DAB converter using MATLAB/Simulink. The simulated system parameters are mentioned in Table VII.

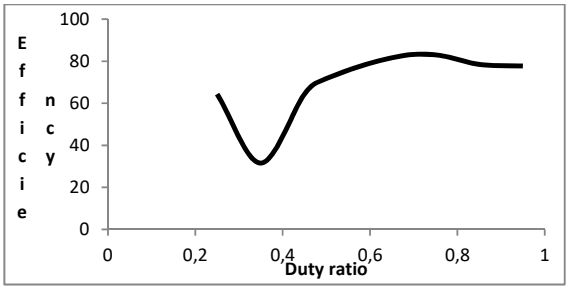

Fig. 19 (a)Graph between efficiency and duty ratio for DAB with EPS control in reverse mode at duty ratio of $D_1 = 0.3$, $D_2 = 0.25$ to 0.95

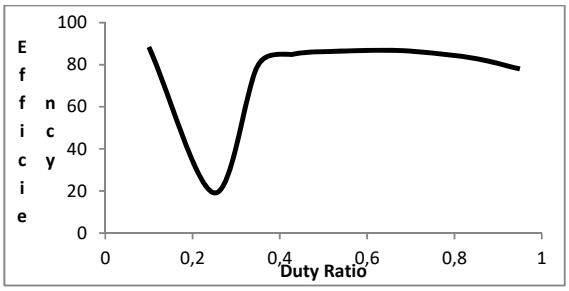

Fig. 19 (b) Graph between efficiency and duty ratio for DAB with EPS control in reverse mode at duty ratio of $D_1 = 0.5$, $D_2 = 0.1$ to 0.95

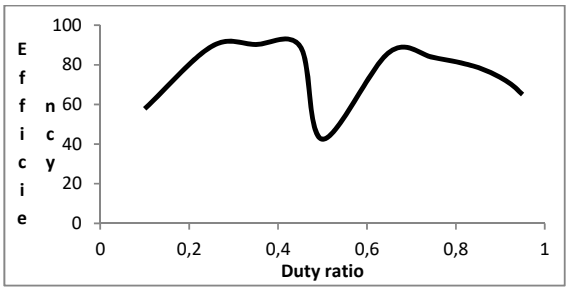

Fig. 19 (c) Graph between efficiency and duty ratio for DAB with EPS control in reverse mode at duty ratio of $D_1 = 0.75$, $D_2 = 0.1$ to 0.90

TABLE VII
SIMULATED SYSTEM PARAMETERS

	SPS (forward)	SPS (reverse)
V_{in} (Input voltage)	302.6 V (HV side)	28.4 V (LV side)
V_{out} (Output voltage)	35.09 V (LV side)	313.2 V (HV side)
C_{in} (Input capacitor)	300 µF	4500µF
C_{out} (Output capacitor)	4500 µF	300 µF
L (Leakage inductor)	450 µH	450 µH
N (Tranformer ratio)	300:100	100:300
SOC (State of charge)	90%	90%
P_{in} (VA)	64	102.7
P_{out} (VA)	45.3	83.8
Efficiency (%)	71.56	81.59

1. Forward Conduction Mode

During the forward conduction mode, the voltage of battery on the HV side is maintained at the voltage of 302 V and the voltage of battery on the LV side is maintained at a voltage of 35.09 V. In forward conduction mode the transformer is having a transformation ratio of 300: 100. During the forward mode of operation, the state of charge (SOC) of the battery on the HV side decreases and it can be seen that the battery is discharging (battery current is having positive value). The above mentioned discharge of battery is shown in the battery characteristics plotted in Fig. 20. During the forward conduction mode, there is increase in SOC of the battery on the LV side and the battery is being charged (battery current is having a negative value). The above mentioned battery characteristics are shown in Fig. 20, through which power flow from HV side to LV side is depicted.

2. Reverse Conduction Mode

In the reverse power flow mode, the voltage of battery on the LV side is maintained at a value of 28.4 V and this serves as the input voltage in reverse conduction mode, and the voltage of battery on the HV side is maintained at a value of 313.2 V. The transformation ratio in this mode is kept at 100: 300. During this mode of operation, a decrement in the SOC of the battery on the LV side can be observed while an increase in the SOC of the battery HV side occurs, thus indicating the power transfer from LV side to HV side. Also the battery on the LV side is discharging (battery current is having a positive value) while that at the HV side is charging (battery current is having a negative value). The above mentioned battery characteristics are shown in Fig. 21, which depicts power flow from LV side to HV side.

The efficiency in both the modes is shown in Table VII, Also the power absorbed and delivered by the batteries are shown in Figs. 22 and 23.

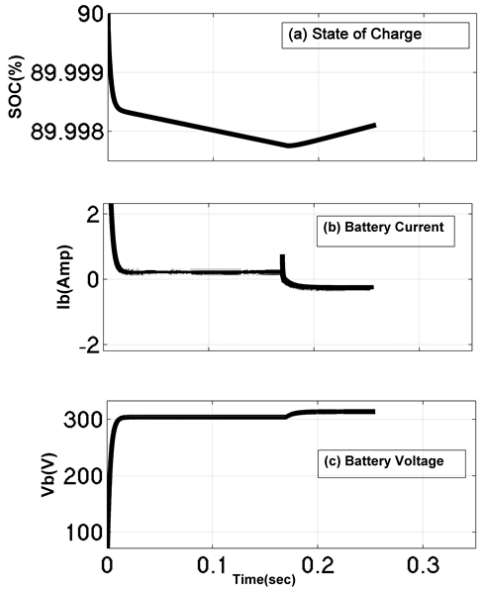

Fig. 20 Battery characteristics showing (a) State of charge of battery (b) Battery current (c) Battery voltage on HV side

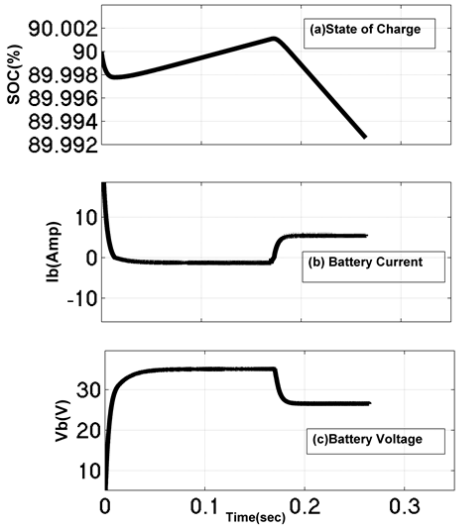

Fig. 21 Battery characteristics showing (a) State of charge of battery (b) Battery current (c) Battery voltage on LV side

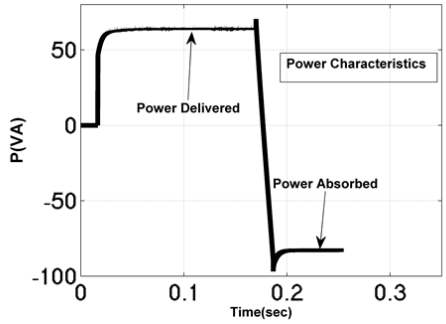

Fig. 22 Power characteristics of battery on the HV side

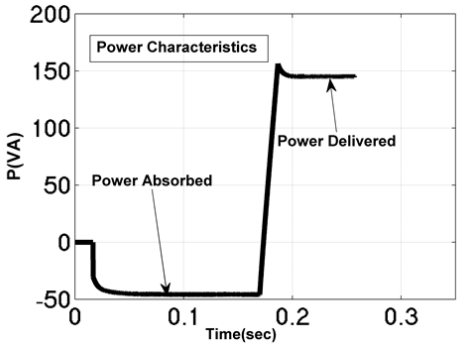

Fig. 23 Power characteristics of battery on the LV side

From Fig. 22, the power characteristics of the battery at the HV side, it is depicted that power is being delivered by the battery in the forward mode, while it is receiving (absorbing) power in the reverse mode. Also from the power characteristics in Fig. 23, it becomes obvious that the battery at the LV side is absorbing power in forward mode and delivering power in reverse mode. Thus, it becomes clear that bidirectional power flow is taking place through the DAB having two lead acid batteries on both the sides in SPS control mode.

B. EPS Technique

The DAB converter in EPS mode is simulated with batteries at both the ends using MATLAB/Simulink and SimPowerSystems software. The system parameters are specified in Table VIII

TABLEVIII
SYSTEM PARAMETERS

	EPS (forward)	EPS (reverse)
V_{in} (Input voltage)	256 V (HV side)	28.85 V (LV side)
V_{out} (Output voltage)	50.08 V (LV side)	275.5 V (HV side)
C_{in} (Input capacitor)	300µF	4500µF
C_{out} (Output capacitor)	4500 µF	300 µF
L (Leakage inductor)	490 µH	490 µH
N (Tranformer ratio)	300:100	100:300
SOC (State of charge)	90%	90%
P_{in} (VA)	267.23	128.97
P_{out} (VA)	258.59	109.65
Efficiency (%)	96.76	85.02

In EPS mode, the voltage of battery on the HV side is maintained at a value of 256 V and the battery on the LV side attains a value of 50.08 V while in reverse conduction mode the voltage on LV side is maintained at 28.85 V and the voltage on HV side achieves a voltage of 275.5 V. The battery characteristics are shown in Figs. 24 and 25.

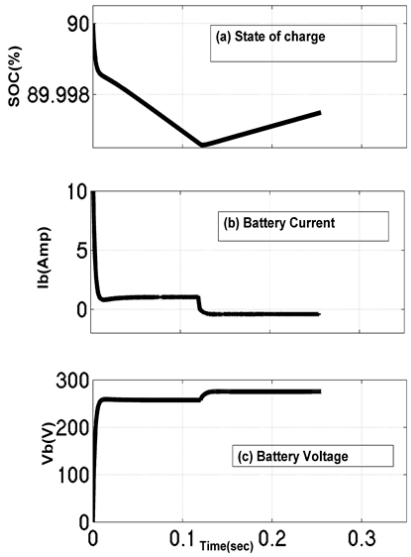

Fig. 24 Battery characteristics showing (a) State of charge of battery (b) Battery current (c) Battery voltage on HV side

1. Forward Conduction Mode

From the characteristics, it can be seen that the battery at the HV side discharges (positive battery current) causing the SOC of the battery on the HV side to decrease (Fig. 24) and the battery at the LV side is getting charged (negative battery current) causing the SOC of the battery to increase (Fig. 25). The transformation ratio during the forward conduction mode is maintained at 300:100

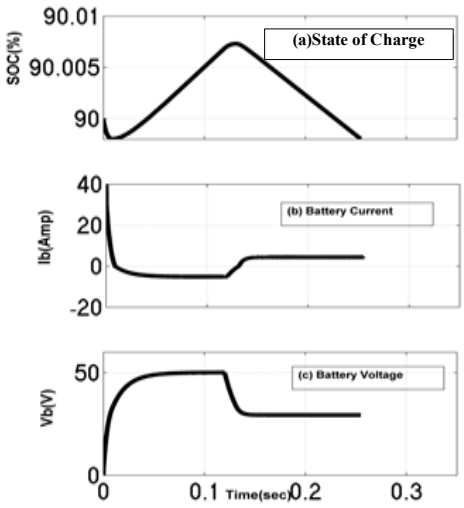

Fig. 25 Battery characteristics showing (a) State of charge of battery (b) Battery current (c) Battery voltage on LV side

2. Reverse conduction Mode

During the reverse conduction mode, the battery at the LV side is discharging (positive battery current) causing the SOC of the battery on the LV side to decrease as this is the input in reverse conduction mode. The SOC of battery on the HV side is increasing and the battery is charging (negative battery current).

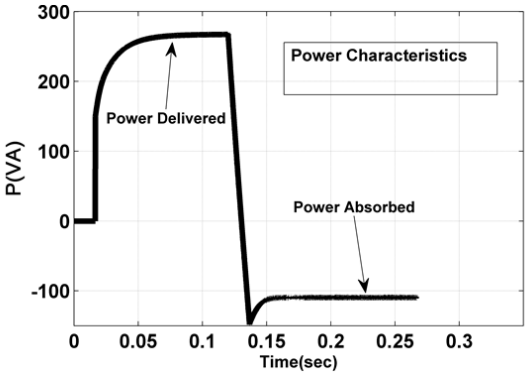

Fig. 26 Power characteristics of battery on the HV side

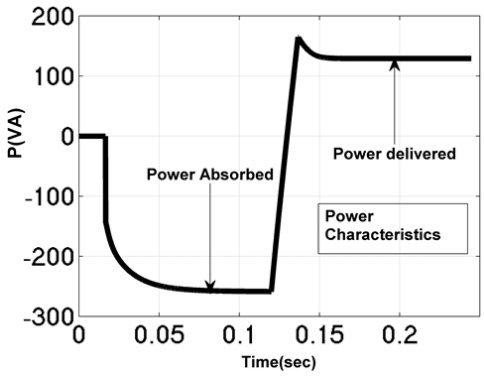

Fig. 27 Power characteristics of battery on the LV side

The efficiency in both the modes is shown in Table VII. Also, the power absorbed and delivered by the batteries is shown in Figs. 26 and 27.

Fig. 26 shows the power characteristics of the battery on the HV side; from the characteristics, it can be easily demonstrated that the battery at the HV side delivers power in the forward mode, and it receives (absorbs) power in the reverse conduction mode. Also from the power characteristics in Fig. 27, it can be clearly manifested that the battery at the LV side absorbs power in the forward conduction mode and delivers power in the reverse conduction mode.

VI. Conclusions

From the analysis of DAB in SPS with reduced rule based fuzzy logic controlled closed loop controller control, it can be concluded that DAB with SPS control when controlled with fuzzy logic controller gives stable operation over the whole operating zone. In the forward mode of operation, power is being transferred from the battery at High Voltage bus to the battery at LV Bus. The maximum efficiency (71.56%) in forward conduction mode is obtained at a duty ratio of 0.02.At this duty ratio, power of 45.8 VA is stored in the battery at the LV side while battery at the HV side is supplying a power of 64 VA while in reverse conduction mode maximum efficiency (81.59%) for converter operation is attained at the duty ratio of 0.82. At this duty ratio power is transferred from the battery at the LV side to the battery at the HV side. In this mode 102.7 VA of power is transferred from the LV side and 83.8 VA of power is stored in the battery on the HV side. After this, the analysis of DAB in EPS control mode with reduced rule based fuzzy logic controlled closed loop controller is done, from which it can be concluded that DAB with EPS control when controlled with fuzzy logic controller also gives stable operation over the whole operating zone. In the forward mode of operation power is being transferred from the battery at High Voltage bus to the battery at Low Voltage bus. As the maximum efficiency (96.70%) in forward mode is obtained at a duty ratio of D_1=0.5, D_2=0.483.At this duty ratio power of 258.7 VA is stored in the battery at the LV side while battery at the HV side is supplying a power of 267.23 VA.

While in the reverse conduction mode maximum efficiency (85.02%) is attained at a duty ratio ofD_1=0.5, D_2=0.43. At this duty ratio, power is transferred from LV side battery to the battery on the HV side. In this mode 128.97 VA of power is transferred from the LV side and 109.65 VA of power is stored in the battery on the HV side.

In the present work, the SOCs of both the batteries are shown along with their respective current. The changes in SOC's (increasing while charging and decreasing while discharging) and the changes in battery current (negative for charging and positive for discharging) make the bidirectional power flow evident.

As only two membership functions are required for linguistic variables in fuzzy logic controller, 4 rule based fuzzy logic controller is developed. Upon application of reduced rule based fuzzy logic controller, waveforms are stable over the whole operating zone and no distortion in

waveforms is observed. Also the converter is operated at optimum duty ratios and the requirement of mathematical model is eliminated. Fuzzy logic controller provides a smooth closed loop control of the dual battery system containing DAB converter. Thus bidirectional power flow is achieved with better efficiency (greater than 85%) for both forward and reverse modes. Thus for bidirectional power flow with batteries, the isolated DC-DC DAB converter with EPS control exhibits a better performance as compared to that with SPS control.

REFERENCES

[1] H. Bai and Mi. C, "Eliminate reactive power and increase system efficiency of isolated bidirectional dual-active-bridge DC-DC converters using novel dual-phase-shift control," *IEEE Trans. Power Electron.,* vol. 23,no. 6, pp. 2905–2914, Nov,2008.

[2] B. Zhao, Q. Song, W. Liu, Y. Sun, (2014) "Overview of Dual-Active Bridge Isolated Bidirectional DC-DC Converter for High Frequency-Link Power Conversion System," *IEEE Trans. Power Electron*, Vol. 29, No.8, pp. 4091-4106, Aug,2014.

[3] S. P. Engel, M. Stieneker, N. Soltau, S. Rabiee, H. Stagge and R. W. De Doncker "Comparison of the Modular Multilevel DC Converter and the Dual-Active Bridge Converter for Power Conversion in HVDC and MVDC Grids" *IEEE transactions on power electronics,* vol. 30, no. 1, January, 2015.

[4] X. Shi, J. Jiang, X. Guo, "An Efficiency-Optimized Isolated Bidirectional DC-DC Converter with Extended Power Range for Energy Storage Systems in Microgrids," *Energies*, pp.27-44,Dec,2012.

[5] Dong-Keun Jeong, H. Kim, J. Baek, Ju-Yong Kim and Hee-Je Kim, "Dual active bridge converter for energy storage system in dc microgrid", in proceed. *IEEE transportation electrification conference* (ITEC. Asia pacific, 1-4 june, 2016).

[6] S. Inoue. and H. Akagi, "A bidirectional isolated dc-dc converter as a core circuit of the next-generation medium-voltage power conversion system", *IEEE Trans. Power Electron.*,vol.22,no.2,pp.535–542, Mar, 2007.

[7] R. W. A. A. D. Doncker, D. M. Divan, and M. H. Kheraluwala,, "A three phase soft-switched high-power-density dc/dc converter for high-power applications," *IEEE Trans. Ind. Appl.*, vol. 27, no. 1, pp. 63–73, Jan./Feb. 1991.

[8] G. E. Sfakianakis, J. Everts, H. Huisman and E. A. Lomonova, "Comparative evaluation of bidirectional dual active bridge dc-dc converter variants", in proceed. *IEEE vehicle power and propulsion conference* (VPPC)-17-20 October, 2016.

[9] S. P. Engel, N. Soltau, H. Stagge and R. W. De Doncker "Dynamic and Balanced Control of Three-Phase High-Power Dual-Active Bridge DC–DC Converters in DC-Grid Applications", *IEEE transactions on power electronics*, vol. 28, no. 4, april,2013 .

[10] A. Filba-Martinez, S. Busquets-Monge, J. Nicolas-Apruzzese and J. Bordonau, "Operating Principle and Performance Optimization of a Three-Level NPC Dual-Active-Bridge DC–DC Converter", *IEEE transactions on industrial electronics*, vol. 63, no. 2, February,2016 .

[11] B. Zhao, Q. Song, J. Li, Y. Wang and W. Liu, "Modular Multilevel High-Frequency-Link DC Transformer Based on Dual Active Phase-Shift Principle for Medium-Voltage DC Power Distribution Application", *IEEE transactions on power electronics*, vol. 32, no.3, march2017.

[12] X. Li and A.K.S. Bhat., "Analysis and design of high-frequency isolated dual-bridge series resonant dc/dc converter," IEEE Trans. Power Electronics, vol. 25, no. 4, pp. 850 862, Apr. 2010.

[13] B. Zhao, Q. Yu and W. Sun (2012) "Extended-Phase-Shift Control of Isolated Bidirectional DC-DC Converter for Power Distribution in Microgrid," *IEEE Trans. Power Electron.,* Vol. 27, No. 11,pp. 4667-4679, Nov,2012.

[14] C. Mi, H. Bai, C. Wang, and S. Gargies "Operation, design and control of dual H-bridge-based isolated bidirectional DC-DC converter", *IET Power Electron.,* Vol. 1, No. 4, pp. 507-517,Ma,2008.

[15] B. Zhao, Q. Song, and W. Liu. "Power Characterization of Isolated Bidirectional Dual-Active-Bridge DC-DC Converter with Dual-Phase Shift Control," *IEEE Transactions on Power Electronics*, vol. 27, pp.4172-4176,2012

[16] H. Wen, W. Xiao, "Bidirectional Dual-Active-Bridge DC-DC Converter with Triple-Phase-Shift Control" in proceed, *applied power electronics conference and exposition (APEC)*, 17-21 may, 2013.

[17] M. Schweizer, Biela, S. Waffler, and W.J. Kolar., "SiC versus Si-Evaluation of potentials for performance improvement of inverter and dc-dc converter systems by SiC power semiconductors," *IEEE Trans. Ind. Electron.*, vol. 58, no. 7, pp. 2872–2882, Jul. 2011.

[18] N. D. Weise, G. Castelino, K. Basu and N. Mohan, "A Single-Stage Dual-Active-Bridge-Based Soft Switched AC–DC Converter With Open-Loop Power Factor Correction and Other Advanced Features", *IEEE Transactions on power electronics*, vol. 29, no. 8, august,2014.

[19] J. Riedel, D. G. Holmes, B. P. McGrath and C. Teixeira, "ZVS Soft Switching Boundaries for Dual Active Bridge DC–DC Converters Using Frequency Domain Analysis", *IEEE transactions on power electronics*, vol. 32, no. 4, april,2017 .

[20] H. Fujita and H. Akagi, "Unified Power Quality Conditioner: the Integration of Series and Shunt Active Filter", *IEEE Trans. Power Electronics,* vol,13, No.2, pp315-322, 1998.

[21] A. Kumar, A.H. Bhat and S.P. Singh, "Performance evaluation of fuzzy logic controlled voltage source inverter based unified power quality conditioner for mitigation of voltage and current harmonics," *2016 International Conference on Advances in Computing, Communications and Informatics (ICACCI)*, Jaipur, pp. 1799-1804,2016.

[22] S.P. Singh, A.H. Bhat, and A. Kumar, "Fuzzy logic based dynamic voltage restorer for addressing various power quality problems," *2016 IEEE 7th Power India International Conference (PIICON)*, Bikaner, pp. 1-5, 2016.

[23] R. Ullah, A. Ali, Z. Ullah, "Zero Voltage Switched Full Bridge Converters for the Battery Charger of Electric Vehicle". World Academy of Science, Engineering and Technology, International Science Index 117, *International Journal of Electrical, Computer, Energetic, Electronic and Communication Engineering*, 10(9), 1183 – 1192,2016.

[24] V. Tejwani, B.Suthar, "Energy Management System in Fuel Cell, Ultracapacitor, Battery Hybrid Energy Storage". World Academy of Science, Engineering and Technology, International Science Index 108, *International Journal of Electrical, Computer, Energetic, Electronic and Communication Engineering*, 9(12), 1492 – 1500,2015.